EJN European Journal of Neuroscience

FENS Federation of European Neuroscience Societies

European Journal of Neuroscience, pp. 1–9, 2015 doi:10.1111/ejn.12969

Topological organization of CA3-to-CA1 excitation

Yoshie Hongo,[1] Koichi Ogawa,[1] Yuji Takahara,[1] Keiko Takasu,[1] Sebastien Royer,[2] Minoru Hasegawa,[1] Gaku Sakaguchi[1] and Yuji Ikegaya[3,4]

[1]Pain & Neuroscience, Discovery Research Laboratory for Core Therapeutic Areas, Shionogi Co. Ltd, Toyonaka, Osaka, Japan
[2]Center for Functional Connectomics, Korea Institute of Science and Technology, Seoul, South Korea
[3]Laboratory of Chemical Pharmacology, Graduate School of Pharmaceutical Sciences, The University of Tokyo, 7-3-1 Hongo, Bunkyo-ku, Tokyo 113-0033, Japan
[4]Center for Information and Neural Networks, National Institute of Information and Communications Technology, Suita City, Osaka, Japan

Keywords: calcium imaging, epilepsy, hippocampus, network, rat, sequence

Abstract

The CA1-projecting axons of CA3 pyramidal cells, called Schaffer collaterals, constitute one of the major information flow routes in the hippocampal formation. Recent anatomical studies have revealed the non-random structural connectivity between CA3 and CA1, but little is known regarding the functional connectivity (i.e. how CA3 network activity is functionally transmitted downstream to the CA1 network). Using functional multi-neuron calcium imaging of rat hippocampal slices, we monitored the spatiotemporal patterns of spontaneous CA3 and CA1 burst activity under pharmacological GABAergic blockade. We found that spatially clustered CA3 activity patterns were transformed into layered CA1 activity sequences. Specifically, synchronized bursts initiated from multiple hot spots in CA3 ensembles, and CA1 neurons located deeper in the pyramidal cell layer were recruited during earlier phases of the burst events. The order of these sequential activations was maintained across the bursts, but the sequence velocity varied depending on the inter-burst intervals. Thus, CA3 axons innervate CA1 neurons in a highly topographical fashion.

Introduction

Hippocampal CA3 neurons are inter-wired (Amaral & Lavanex, 2007) and constitute an auto-associative network that is theoretically implicated in associative memory and pattern completion (Hopfield, 1982). Recent evidence has demonstrated that CA3 output is involved in associative learning and memory consolidation (Nakashiba *et al.*, 2008, 2009). CA1 pyramidal cells are major distal targets of CA3 pyramidal cells. An axonal tracer study has demonstrated that the spatial pattern of the CA3-to-CA1 projections is not random; proximal CA3 neurons project preferentially to CA1 neurons at levels septal to their location, whereas distal CA3 neurons project preferentially to temporal CA1 neurons (Ishizuka *et al.*, 1990) (for topographical items, see Fig. 1). A sophisticated genetic study has recently revealed that the axons of CA3 neurons create synapses more heavily onto a fraction of the dendritic branches of CA1 neurons (Druckmann *et al.*, 2014), suggesting that the CA3-to-CA1 connectivity is organized at the subcellular level.

Compared with the anatomical structure, the functional connectivity (i.e. the activity propagation patterns) of the hippocampus has not been as well characterized. Its functional connectivity is not necessarily identical to the structural connectivity because the strengths of individual synapses are inhomogeneous and even modifiable (Sasaki *et al.*, 2012). Additionally, a significant proportion of synapses are functionally silenced in the hippocampus (Liao *et al.*, 1995).

Elucidating the activity flow patterns requires functional recording from living neuronal networks. Here, we focused on synchronized burst activity in acute hippocampal slices. The slices perfused with bicuculline (a $GABA_A$ receptor antagonist) in Mg^{2+}-free artificial cerebrospinal fluid (aCSF) induced epileptiform bursts in the CA1 and CA3 regions (Fig. 2A). The synchronized bursts in CA3 preceded the CA1 bursts by approximately 10–20 ms, and the surgical incision of Schaffer collaterals abolished the CA1 bursts but not the CA3 bursts (Fig. 2B and C). Thus, bursts were initiated in the CA3 region and propagated to the CA1 region. In individual burst events in the CA1 region, the activity of more proximal electrodes occurred earlier than that of more distal electrodes (Fig. 2D). Linear regression analysis between the burst onset times and the recorded locations revealed that the correlation coefficient R was 0.55 (Fig. 2E, $P = 2.7 \times 10^{-14}$, Spearman's rank correlation coefficient), indicating that a burst propagated from the CA1 proximal end to the distal end at a velocity of 69 ± 9 mm/s (horizontal propagation; mean $\pm$ SD of 161 electrodes in three slices). This activity propagation pattern along the stratum pyramidale was less evident in the bursts in the CA3 region (Fig. 2F, $R = -0.07$, $P = 0.51$). These data suggest that the initiation and propagation mechanisms underlying synchronous bursts differ between the CA3 and CA1 networks. Therefore, in this study we monitored the spatiotemporal patterns of

Correspondence: Yuji Ikegaya, [3]Laboratory of Chemical Pharmacology, as above.
E-mail: ikegaya@mol.f.u-tokyo.ac.jp

Received 26 February 2015, revised 7 May 2015, accepted 28 May 2015

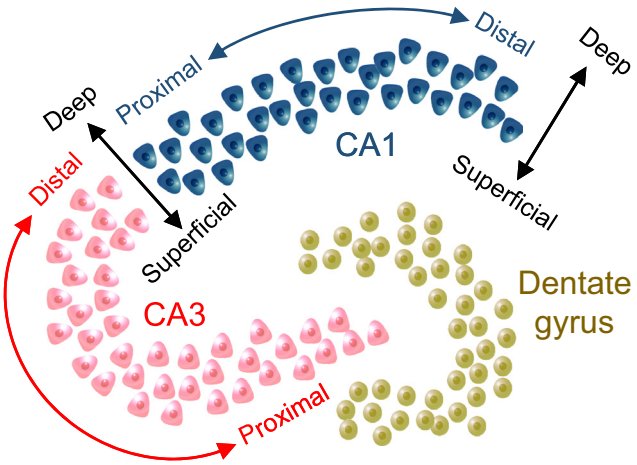

FIG. 1. Schematic illustration of the topographical elements of the hippocampus. The terms proximal and distal indicate the relative distance from the dentate gyrus along the stratum pyramidale. For example, a more proximal CA1 neuron is located closer to CA3. The terms superficial and deep indicate the relative distance from the stratum radiatum across the stratum pyramidale. For example, a deeper CA1 pyramidal cell is located closer to the stratum oriens.

these bursts using a functional multi-neuron imaging technique with cellular resolution.

Materials and methods

Animal experiment ethics

The experiments were performed using Wistar rats of either sex (6–8 days old) (SLC, Shizuoka, Japan). The rats were housed in a temperature- and humidity-controlled environment with a 12-h light/dark cycle and were allowed *ad-libitum* access to water and food. All procedures were approved by the Animal Care and Use Committee of Shionogi Research Laboratories (Osaka, Japan) in agreement with internal guidelines for animal experiments and in adherence with the ethics policy of Shionogi Co., Ltd (Osaka, Japan).

Slice preparations

The rats were decapitated, and the brains were quickly removed and immersed in ice-cold sucrose-based physiological saline consisting of (in mM): 25 $NaHCO_3$, 1.0 NaH_2PO_4, 3.0 KCl, 5.0 $MgCl_2$, 1.0 $CaCl_2$, 11 glucose, and 215.5 sucrose, bubbled with 95% O_2 and 5% CO_2. The hippocampus was isolated and embedded in 3% agarose gel. Transverse hippocampal slices (400 μm) were cut using a vibratome (VT1200S; Leica, Wetzlar, Germany). The slices were maintained for more than 40 min at 32 °C in aCSF consisting of (in mM): 113 NaCl, 25 $NaHCO_3$, 1.0 NaH_2PO_4, 3.0 KCl, 1.0 $MgCl_2$, 2.0 $CaCl_2$, and 11 glucose, bubbled with 95% O_2 and 5% CO_2.

Calcium imaging

To load the cells with Oregon Green 488 BAPTA-1AM, the slices were incubated for 60–80 min at 32 °C with 0.0005% Oregon Green 488 BAPTA-1AM (Invitrogen, Carlsbad, CA, USA), 0.01% Pluronic F-127 (Invitrogen), and 0.005% Cremophor EL (Nacalai Tesque, Kyoto, Japan). After a recovery period of at least 40 min in aCSF, the slices were transferred to a recording chamber perfused with Mg^{2+}-free aCSF, which contained (in mM): 113 NaCl, 25 $NaHCO_3$, 1.0 NaH_2PO_4, 3.0 KCl, 2.0 $CaCl_2$, and 11 glucose, bubbled with 95% O_2 and 5% CO_2, at a rate of 2.0 mL/min at 30–32 °C, unless otherwise noted. Recordings were obtained from slices that had been continuously perfused with 10 μM (-)bicuculline methobromide (Wako, Osaka, Japan). Time-series confocal images were captured for 24 min at 33 frames/s using a Nipkow-disk confocal unit (CSUX1; Yokogawa Electric, Tokyo, Japan) with a cooled CCD camera (iXon DU897; Andor Technology, Belfast, UK) attached to an upright microscope (Eclipse FN1, Nikon, Tokyo, Japan), with a water-immersion objective (16×, 0.80 numerical aperture; Nikon) and image acquisition software (Andor iQ; Andor Technology). Oregon Green 488 BAPTA-1AM was excited at 488 nm through a 5% neutral density filter with a laser (30 mW, BC-001-B; Melles Griot, Albuquerque, NM, USA). The cell bodies of individual neurons were identified visually, and the regions of interest were determined, in which the average fluorescence was measured. To exclude sampling bias, the slices with more than 80 regions of interest were used for the analyses. For each region of interest, the change in somatic fluorescence ($\Delta F/F$) was calculated as $(F_1 - F_0)/F_0$, where F_1 is the fluorescence intensity at any time-point and F_0 is the average baseline fluorescence intensity over ±15 s. The spikes were reconstructed using custom software written in Microsoft Visual Basic (Sasaki *et al.*, 2008). To evoke synchronous activity, 200-μs electrical pulses were applied at an interval of 5–90 s through bipolar tungsten electrodes (Inter Medical Co., Ltd, Aichi, Japan) using a stimulator (SEN-3401; Nihon Kohden, Tokyo, Japan) and an isolator (SS-203J; Nihon Kohden). The stimulus intensity ranged between 0.1 and 3 mA and was set at a level that could activate at least 90% of neurons in the imaged field.

Electrophysiology

The CA1 or CA3 pyramidal cells were visually identified and targeted for loose patch cell-attached recordings or local field potential recordings using borosilicate glass pipettes filled with aCSF (2–6 MΩ). Data were obtained using an EPC10 amplifier (HEKA, Darmstadt, Germany) and Pulse software (HEKA), with a low-pass filter at 2.9 kHz. The signal was digitized at 10 kHz using PowerLab (ADInstruments, Dunedin, New Zealand) and then analysed using LabChart software (ADInstruments). In experiments using multi-electrode arrays, hippocampal slices were placed in a recording chamber with an array of 64 planar multi-electrodes (ϕ = 50 μm, MED-P50025; Alpha MED Scientific, Inc., Osaka, Japan). Local field potentials were recorded using a multi-channel recording system (Cerebus Data Acquisition System, Blackrock Microsystems, Salt Lake City, UT, USA) with a band-pass filter of 0.3–500 Hz and then digitized at 10 kHz using Central software (Blackrock Microsystems).

Statistics

Data were analysed using GraphPad Prism (GraphPad Software, San Diego, CA, USA) and custom software written in Matlab (MathWorks, Natick, MA, USA). Unless otherwise noted, data are presented as the mean ± SD. Significance was set at $P < 0.05$. To evaluate the sequence fidelity (event-to-event consistency in order of the neuronal sequences), we adopted Kendall's coefficient of concordance (W), an indicator of the rank consistency (Kendall *et al.*, 1994). W consists of a value between 0 and 1; a higher value corresponds to a higher consistency. To assess the correlation between the activity onset and the cell location (i.e. the distance from the

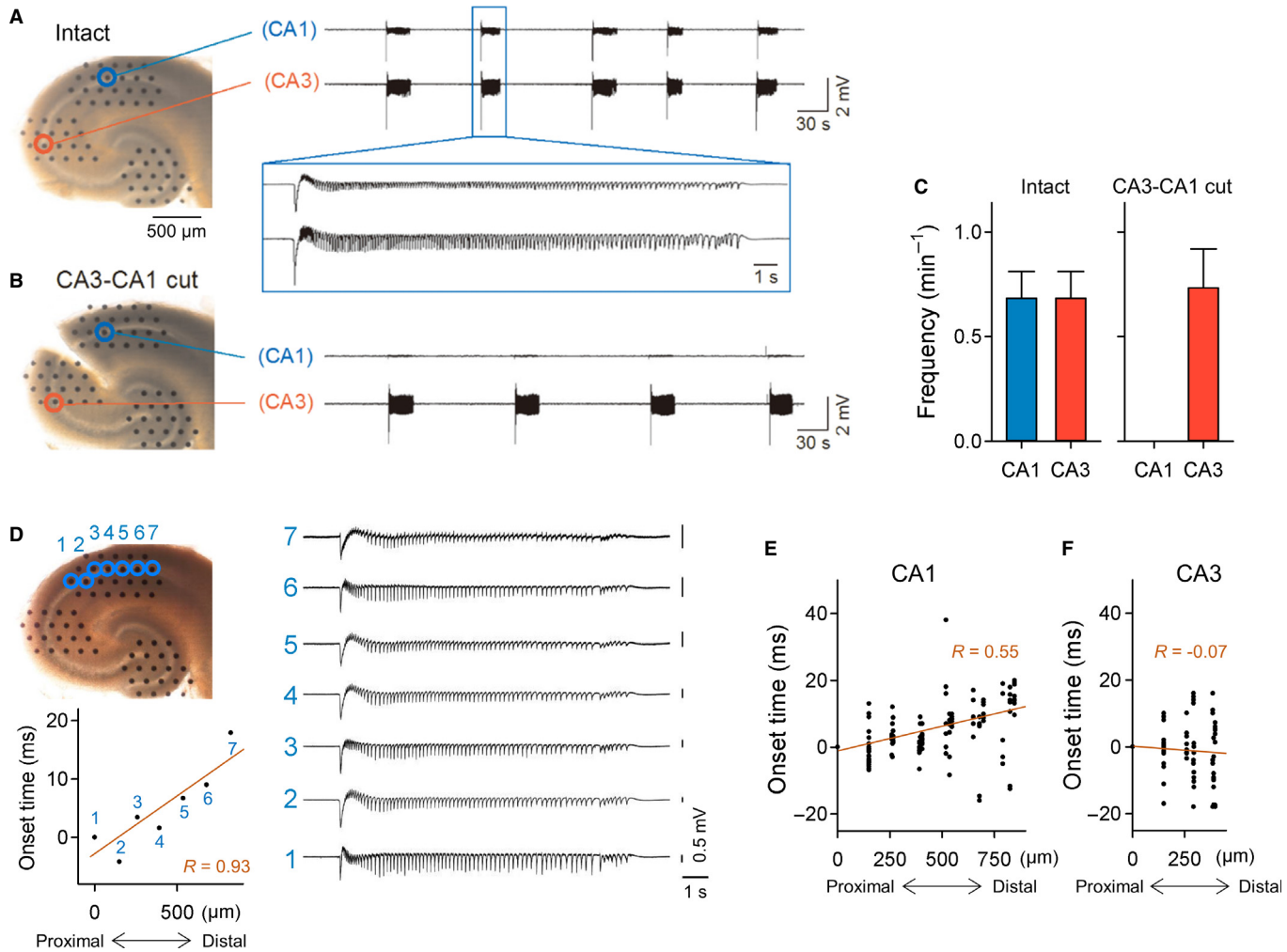

FIG. 2. Synchronized bursts occurring spontaneously in disinhibited hippocampal slices: multi-channel local field potential (LFP) recordings. (A) Multi-electrode recordings of CA1 and CA3 neuronal activity from acute hippocampal slices treated with 10 μM bicuculline under Mg^{2+}-free conditions. LFPs of spontaneously occurring bursts were synchronized between CA1 and CA3. (B) The same as A, except that a slice received a surgical incision between the CA3 and CA1 regions (CA3–CA1 cut). (C) The event frequency of synchronous activity in the CA1 and CA3 regions in intact slices (left) and slices with a CA1–CA3 cut (right) is shown as the mean ± SEM of three slices each. (D) Regression analysis of a single burst in a representative slice. The onset times in a burst (right) recorded from seven electrodes close to the CA1 pyramidal cell layer (left top) are plotted against the Euclidean distance from the electrode located closest to CA3 (left bottom). (E) Data were pooled from all 23 bursts recorded from a total of 161 electrodes in three slices. The best linear fit revealed that the correlation coefficient R was 0.55 ($P < 0.0001$), indicating that synchronized bursts propagated from the proximal to distal ends of CA1. (F) The same as in E, except for CA3.

border between the stratum oriens and pyramidale), we adopted Spearman's rank order correlation coefficient. The Z-test for two correlation coefficients was used to evaluate the difference between the coefficients (Kendall *et al.*, 1994). To classify the time compression and expansion of sequential activation, we employed a resampling method and produced 1000 surrogate datasets that provided the chance distribution.

Results

Layer-patterned, sequential CA1 neuron activation

The local field potential recordings revealed that hippocampal slices were disinhibited by bicuculline and generated synchronized bursts at a mean ± SD frequency of 0.68 ± 0.22/min (Fig. 2A and C; n = 3 slices). These bursts were imaged from the CA1 stratum pyramidale of Oregon Green 488 BAPTA-1AM-loaded slices (Fig. 3A). In single movies, we monitored an average of 146 ± 29 neurons (Fig. 3B, mean ± SD of 32 slices). The neurons emitted spontaneous elevations in Ca^{2+} concentration that reflected action potentials, and synchronized bursts induced larger and more prolonged Ca^{2+} increases than sporadic spikes (Fig. 3A). Each burst event recruited 99.9 ± 0.3% of the neurons (Fig. 3C, mean ± SD of 193 events from 10 slices). Sporadic activity was maintained at a low level after the occurrence of the first burst event (Fig. 3C), and it was further suppressed transiently after every burst (Fig. 3D). This transient silencing of network activity may result from depletion of the releasable glutamate pool after prolonged epileptic discharges of hippocampal networks (Staley *et al.*, 1998). Thus, the bursts represent almost fully synchronized, epileptiform network events. No synchronized bursts were observed in the CA1 regions independently from those in the CA3 region (Fig. 3E and F, n = 4 slices each).

Neurons were not completely synchronized within a single burst event. Rather, they were sequentially activated at various times over approximately 100 ms. Although the activation orders of individual neurons were not strictly preserved across events, they seemed to be

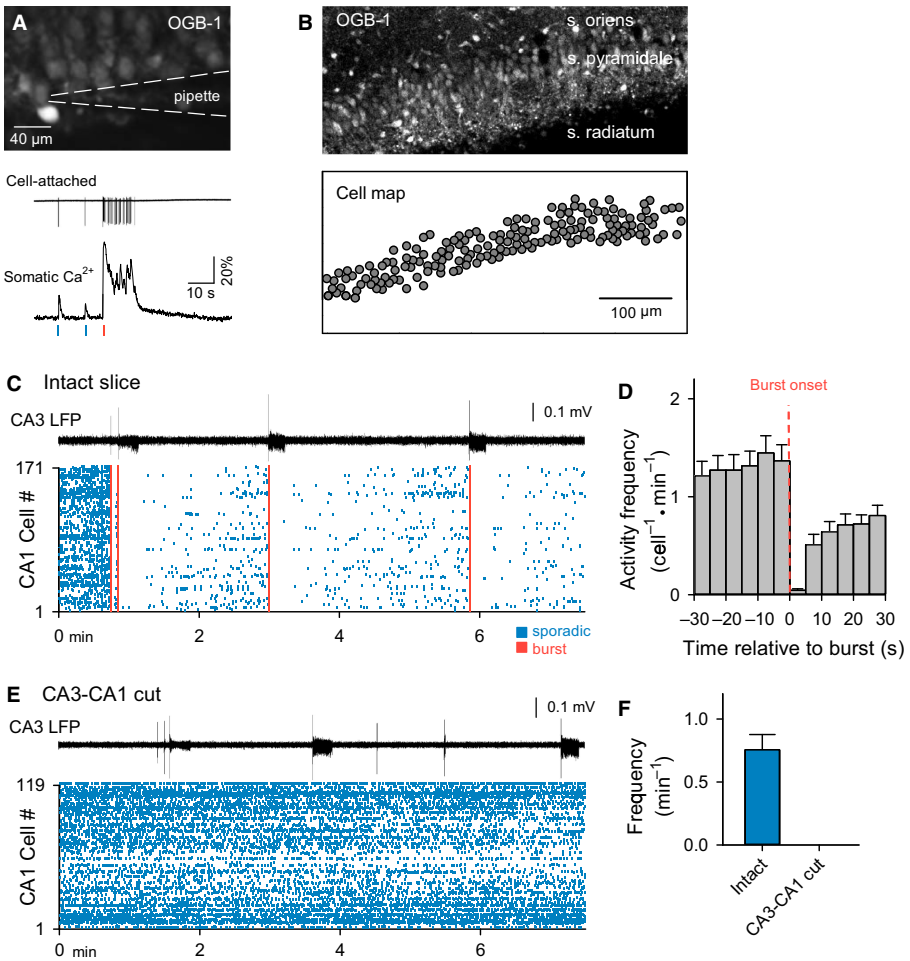

FIG. 3. Synchronized bursts in disinhibited hippocampal slices: functional multi-neuron calcium imaging. (A) A confocal snapshot of the CA1 region of an Oregon Green 488 BAPTA-1AM (OGB-1)-loaded slice (top). The dashed lines indicate the position of a pipette used for cell-attached recordings. Spikes were associated with somatic calcium elevations (bottom). The blue and red lines indicate sporadic and bursting spikes, respectively. (B) A representative OGB-1 fluorescence image of the CA1 stratum pyramidale (top) and the locations of a total of 171 monitored neurons (bottom). (C) A rastergram of the calcium activity of individual CA1 neurons in a disinhibited intact slice. The blue and red lines indicate sporadic spikes and synchronized bursts, respectively. The traces above the rastergram are local field potentials (LFPs) recorded simultaneously from the CA3 stratum pyramidale, indicating that the synchronous CA1 bursts occurred together with the CA3 bursts. (D) The burst event-triggered average of spike activity in all CA1 neurons. Data are shown as the means ± SEMs of 30 bursts in four slices. (E) The same as in C, except for a disinhibited slice with a CA3–CA1 cut. (F) The event frequency of synchronous activity in the CA1 region in intact slices and slices with a CA1–CA3 cut are shown as the means ± SEMs of four slices each.

loosely maintained as a whole (Fig. 4A). Thus, we analysed the activation timings in a total of 193 burst events recorded from 10 slices (12–37 events per slice). Within individual slices, the overall orders of the neuronal activations were roughly maintained across bursts; Kendall's coefficients of concordance were statistically significant in all slices, ranging between 0.13 and 0.42 ($\chi^2 = 326$–1392, $P = 8.2 \times 10^{-215}$–1.9×10^{-15}). For each burst event, we counted the number of neurons activated in single imaging frames (a 30-ms bin) and determined the synchronization peak time (i.e. the frame in which the maximal number of coactive neurons was observed). For each slice, we pooled data from all observed bursts and obtained the time histogram of the total activity level relative to the synchronization peak time. In this event-triggered average histogram, we determined the mean activation timings of the individual neurons and displayed them in a timing map format (Fig. 4B). The timing map of a representative slice is shown in Fig. 4B, indicating earlier activation of the cells located closer to the stratum oriens (deeper stratum pyramidale). This tendency held true for the data pooled from all 1444 cells in 10 slices (Fig. 4C). The activation timing was negatively correlated with the distance from the border between the stratum oriens and pyramidale ($R_{rank} = 0.61$, $P = 3.6 \times 10^{-147}$), indicating that the activity propagated vertically from deep neurons to superficial neurons in the CA1 stratum pyramidale. Regression analysis revealed that the velocity of the vertical propagation was 2.2 ± 0.1 mm/s (mean ± SD of 10 slices) and was approximately 30-fold slower than the horizontal propagations recorded using multi-electrode arrays (Fig. 2E; cf. 69 ± 9 mm/s).

To examine whether this layered pattern of neuron activation was due to differences in the excitability of CA1 cells, we artificially activated the CA1 neurons. The CA1 regions were surgically isolated from the CA3 network (i.e. a CA1–CA3 cut), and the stratum radiatum was field-stimulated every 5–90 s using a bipolar electrode (Fig. 5A). The stimulation activated 99.0 ± 1.4% of the neurons per stimulus (mean ± SD of 80 stimuli in eight slices). Kendall's coefficients of concordance for stimulation trials ranged between 0.095 and 0.358 and reached the level of significance ($P < 0.05$) in five of eight slices, indicating that the activation orders of the individual neurons were roughly preserved across the stimulation trials. However, within the pooled data, the correlation coefficient R_{rank} between the activation time and the distance from the stratum oriens

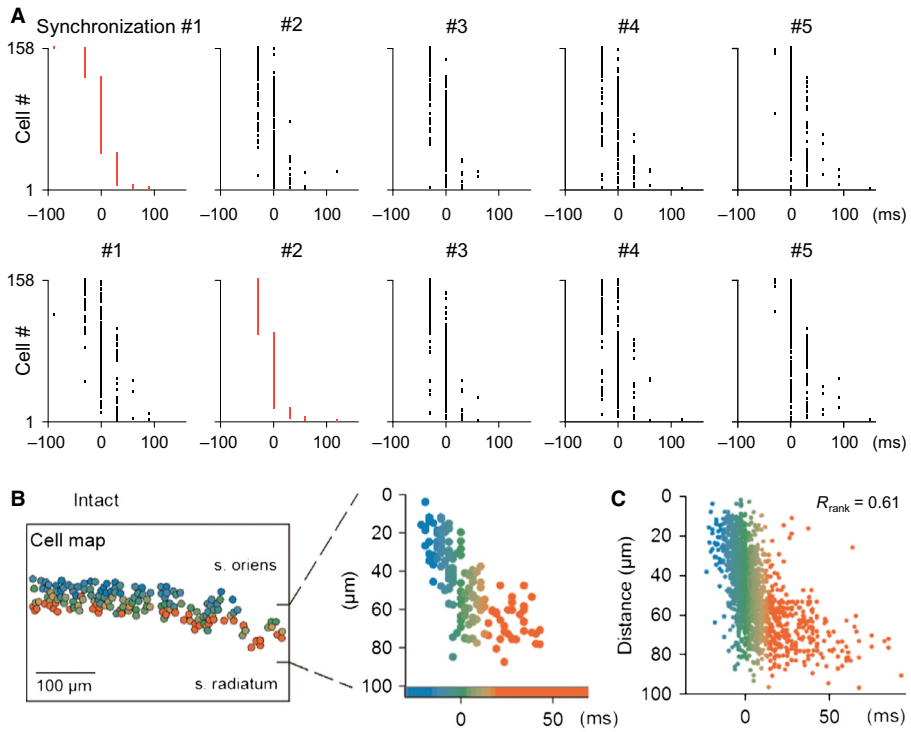

FIG. 4. Layered activation of CA1 neurons during synchronized bursts. (A) Sequential neuron activation during bursts in a representative slice. The onset times of calcium transients in 158 individual cells are compared between the first five synchronized burst events. The onset times are aligned relative to those observed in the first (top) and second (bottom) events. The activation orders were roughly preserved across the events. (B) The 14 bursts in the slice shown in A are summarized in a cell map. The colors of individual cells in the left map indicate the mean activation times relative to the synchrony peak. In the right panel, the same data are shown in a scatter-plot of the timing vs. the distance from the border between the stratum oriens and pyramidale. (C) Data are pooled from a total of 1444 neurons in 10 slices. A negative correlation was found (R_{rank} = 0.61, $P = 3.6 \times 10^{-147}$).

was 0.18, which was significantly lower than the value of 0.61 that was observed in spontaneously synchronized bursts ($Z = 13.5$, $P = 8.4 \times 10^{-42}$, Z-test for two correlation coefficients). These results indicate that the stimulation experiments were unable to replicate the layered activation pattern observed in spontaneous bursts. Therefore, layered activation is unlikely to be due to differences in the intrinsic excitability, but it may emerge from circuit-level dynamics that result from CA3 network activity patterns.

To further confirm this hypothesis, we stimulated Schaffer collaterals in slices that had not been subjected to a CA3–CA1 cut. We perfused these CA3-preserved, intact slices with bicuculline in normal aCSF (containing 1 mM Mg^{2+}). The slices exhibited few spontaneous bursts but responded to field stimulation with synchronized activity (Fig. 5B). Note that these evoked bursts involved direct CA1 activation through Schaffer collateral inputs and indirect CA1 activation through antidromic recruitment of CA3 neuron populations. Thus, these bursts partly reflected the activity dynamics generated in CA3 recurrent networks. In all six slices, Kendall's coefficients of concordance reached the level of significance (ranging between 0.19 and 0.35), and the R_{rank} recovered to 0.32, which was greater than that in the slices with the CA3–CA1 cut ($Z = 3.42$, $P = 6.2 \times 10^{-4}$ vs. stimulation in CA1–CA3 cut slices, $n = 926$ cells). Together, the CA3 ensemble dynamics were likely to give rise to non-randomly sequenced CA1 activation.

Cluster-patterned CA3 neuron activation

We conducted the same analyses for CA3 neuron populations. A total of 188 synchronized bursts (10–47 events per slice) were imaged from 808 cells in the CA3 stratum pyramidale in eight slices (104 ± 15 neurons per slice). In all eight slices, Kendall's coefficients of concordance were statistically significant (ranging between 0.10 and 0.18, $\chi^2 = 140$–866, $P = 2.7 \times 10^{-121}$–4.1×10^{-4}). Thus, CA3 neuron activation was also sequential, and the order was roughly maintained as a whole across the bursts. Unlike the CA1 region, however, a layered structure was not present in the CA3 region (Fig. 6A). Indeed, the R_{rank} was 0.16 (Fig. 6B), which was significantly lower than the value of 0.61 observed in the CA1 region ($Z = 12.48$, $P = 9.7 \times 10^{-36}$). Interestingly, neurons activated earlier seemed to be spatially clustered, forming several "hot spots" in the CA3 stratum pyramidale (Fig. 6A). To examine the existence of these hot spots, we selected the earliest 5% neurons in the total distribution of activation timings and computed their cell-to-cell distances between all possible pairs. The distances between the neurons activated earlier were shorter than those of the total neuron population (Fig. 6C; 5% vs. all: $D = 0.28$, $P = 4.6 \times 10^{-6}$; Kolmogorov–Smirnov test). We then separated the neurons into each 5% bin in the total distribution of activation timings and plotted their D statistics, according to the Kolmogorov-Smirnov test. The D-value was high only for the earliest 5% neuron population (Fig. 6D), indicating that only the neurons activated at the earliest phase were spatially clustered. Thus, CA3 synchronized bursts were initiated in the neuron groups that resided in close proximity with each another.

Temporal flexibility of sequential activation

To evaluate the temporal stability of sequential activation, we examined the event-to-event variability. In the left panels of Fig. 7A, the activation timings of individual CA1 neurons were compared

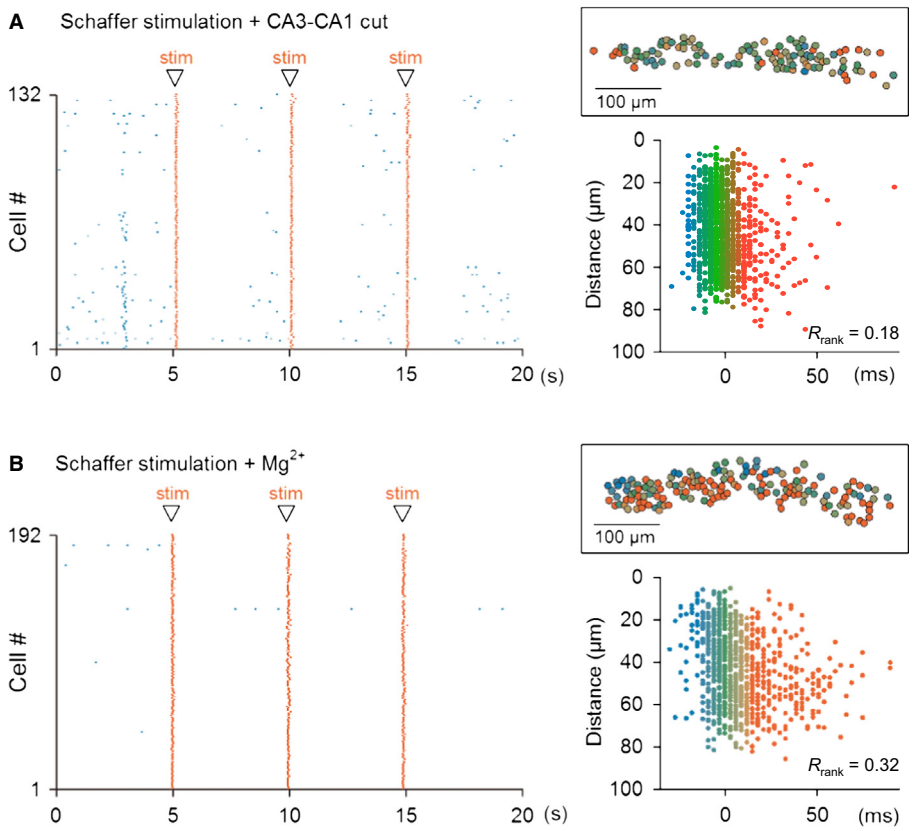

FIG. 5. A lack of sequential activation in stimulation-evoked synchronized events. (A) In disinhibited slices with a CA3–CA1 cut, the CA1 neurons were activated by field stimulation of the Schaffer collaterals. The left rastergram indicates representative activity patterns. The red dots indicate evoked activity. The timing map is shown in the right top inset. The right bottom plot summarizes 1198 neurons in eight slices (R_{rank} = 0.18, $P = 1.0 \times 10^{-9}$). (B) The same as in A, except that intact slices were perfused with bicuculline in 1 mM Mg^{2+} (R_{rank} = 0.32, $P = 6.9 \times 10^{-23}$, n = 926 neurons from six slices).

between two synchronous bursts (events #1 and #9) in an example slice. In the right panels, the activation timings of all 127 neurons were plotted in a pairwise format of event #1 vs. event #9. The correlation coefficient R was 0.45, which was significantly greater than zero ($P = 9.0 \times 10^{-8}$; Spearman's rank correlation coefficient). Figure 7B demonstrates the distribution of the R-values for a total of 2064 pairs of 193 burst events in 10 slices. Among the 2064 pairwise comparisons, 1986 (96.2%) pairs showed significant correlations. These results confirm again that the sequences of CA1 neuronal activation were roughly maintained across burst events, although they were not exact sequence repetitions.

In these regression analyses, we perceived that the slopes of the regression lines varied across pairs. In an example case from Fig. 7A, the slope computed using the least-square fitting methods was 0.45, which is <1. This indicates that the sequence of event #9 occurred more rapidly than that of event #1. We repeated the same analyses for a total of 15 burst events in this slice, and we plotted a 15 × 15 matrix of regression-line slopes (Fig. 7C). Each row pixel of this matrix indicates whether the sequence of the corresponding event was time-compressed (faster) or time-expanded (slower) relative to the compared sequences.

In general, if n burst events are observed in a given slice, $n - 1$ slopes are obtained against the other events. To statistically test whether the distribution of these $n - 1$ values was significantly lower (faster) or higher (slower) than 1 (average), we computed the t-values for a population mean, as follows: $t = (x_i - \mu_0) \times n^{1/2}/s$, where x_i represents the mean slope in a given row i in a slope matrix, and μ_0 and s represent the mean and SD of the total distribution of slopes in the matrix (Kendall *et al.*, 1994). As an example, the t-values of the 15 events analysed in Fig. 7C are plotted in Fig. 7D. For this plot, the 1% significance levels were determined in the chance distribution that was estimated from 1000 surrogates (Fig. 7E). A surrogate was created by random exchanges of all slopes in the slope matrix. In this case, five events (synchronizations #1, #3, #5, #6, and #15) were found to be time-expanded, whereas two events (#4 and #9) were found to be time-compressed. Figure 7F summarizes the type distribution of 191 burst events in 10 slices. The time-compressed, normal, and time-expanded event frequencies were not uniform ($\chi^2_{[2]} = 11.1$, $P = 0.004$). To examine the determinants underlying the sequence velocity of events, we calculated the inter-event time intervals between the focused events and their preceding events. Events that followed longer silent periods were more likely to be time-compressed [Fig. 7G; $F_{2,178} = 13.0$, $P = 5.5 \times 10^{-6}$; compression vs. normal ($Q = 2.82$, $P = 0.01$); Dunnett's multiple comparison test after one-way ANOVA], whereas events that appeared sooner after the previous events were more likely to be time-expanded (expansion vs. normal, $Q = 2.80$, $P = 0.011$).

Discussion

In the present study, we pharmacologically isolated excitatory synaptic activity in acute hippocampal slices. These disinhibited slices repetitively emitted spontaneous synchronized bursts, which propagated from the CA3 region to the CA1 region and were organized in space and time. Thus, they provide a unique platform to study

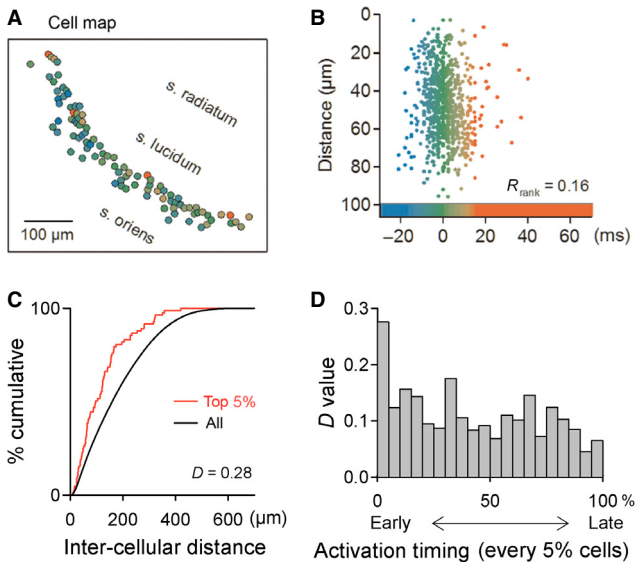

FIG. 6. Burst-initiating spots in CA3 pyramidal cell layers. (A) Synchronized bursts were imaged from the CA3 region in a disinhibited slice, and the activation timings of individual neurons are shown in a pseudocolored scale. (B) Data are summarized from 808 neurons in eight slices (R_{rank} = 0.16, P = 7.8 × 10^{-6}). (C) Cumulative distribution of the distances between all possible pairs of neurons with activation timings during the synchronous events in the earliest 5% (top 5%, red) and 100% (all) of neurons, indicating that the neurons that were activated at earlier phases were located closer to each another (5% vs. all, D = 0.28, P = 4.6 × 10^{-6}; Kolmogorov–Smirnov test). (D) The D-values in the Kolmogorov–Smirnov test are plotted against every 5% neuron population, from the earliest to the latest. Only the neurons activated at the earliest phase were spatially clustered.

CA3-to-CA1 connectivity without contamination from the influences of GABAergic networks. Using this experimental model, we discovered that synchronized bursts were sparsely initiated from multiple hot spots in CA3 ensembles and, thereafter, recruited in deep CA1 neurons during the early phase and superficial CA1 neurons during the late phase of the burst events. The velocities of these neuronal sequences were lower than those of the proximal-to-distal propagations of the activity, and they varied depending on the preceding burst-free periods.

Recent evidence shows that CA1 pyramidal cells are composed of at least two distinct cell types: regular-spiking types and burst-spiking types (Graves *et al.*, 2012). An *in vivo* study has suggested that burst-spiking neurons reside preferentially in the deep sublayer of the CA1 stratum pyramidale (Mizuseki *et al.*, 2011). Most of the CA1 pyramidal cells in the superficial sublayer are immunopositive for calbindin (Baimbridge *et al.*, 1991), a calcium-binding protein that may buffer synaptic Ca^{2+} dynamics (Schmidt, 2012). These neurons also contain high levels of Zn^{2+} (Slomianka, 1992), which may inhibit synaptic *N*-methyl-D-aspartate receptor activity (Ueno *et al.*, 2002). Therefore, these intrinsic properties might explain the various timings of CA1 neuron activation during synchronized bursts; it is possible that superficial CA1 neurons are less excitable because of the presence of calbindin and Zn^{2+} and thereby behave as slow responders during synchronous bursts. To address this possibility, we conducted experiments in which CA1 afferents were artificially stimulated in the absence of CA3 networks. In the artificially evoked events, superficial CA1 neurons did not slow responses. This result is consistent with reports that have demonstrated that the calbindin immunopositivity of CA1 neurons is not correlated with their spiking patterns (Baimbridge *et al.*, 1991) and that regular-spiking and burst-spiking CA1 neurons do not differ in their first spike threshold (Graves *et al.*, 2012). Thus, we conclude that the layered structure in synchronous sequences does not result from a difference in intrinsic properties; instead, it emerges from the CA3-to-CA1 network properties.

The CA1 pyramidal cells in the deep and superficial sublayers are not only heterogeneous in their electrical and morphological properties but also differ in terms of their extrahippocampal inputs (Mizuseki *et al.*, 2011; Scheffer-Teixeira *et al.*, 2012) and subcortical outputs (Sorensen *et al.*, 1993). In addition, our observations suggest that early activated CA3 neurons are spatially clustered and project preferentially to deep CA1 pyramidal cells. Thus, deep and superficial neurons are located in distinct hippocampal circuits and play functionally different roles in information processing. Intriguingly, deep CA1 neurons are more likely to convey spatial information *in vivo*, and a specific fraction of these neurons emit more spikes associated with ripples (Mizuseki *et al.*, 2011). Ripples are synchronized spike complexes with high-frequency field oscillations that primarily originate from the CA3 region and have been associated with the spontaneous reactivation of a recently acquired memory or place cells (Lee & Wilson, 2002). Together with our results, it is possible that behavioral experiences are preferentially encoded in spatially clustered CA3 neurons, which then act as hot spots to trigger ripples. Place cells become activated in sequence as animals pass through distinct locations in a maze, and these sequences are often replayed during ripples, either in forward or reverse order (Lee & Wilson, 2002; Diba & Buzsaki, 2007). The cell sequences are partially preconfigured because they can be detected during sleep prior to the first exploration of an environment (Dragoi & Tonegawa, 2011). The replay of sequences is believed to be critical for learning and memory of reward locations (Girardeau *et al.*, 2009; de Lavilleon *et al.*, 2015); however, the underlying mechanisms are still unclear. The present results demonstrate an intrinsic network bias for sequential activity to be initiated and terminated in anatomically distinct parts of CA3 and CA1. A similar shift in cell activity may occur during ripple-associated place cell sequences, with deep CA1 cells reactivating first and being followed by superficial CA1 cells. Considering that cells encoding reward locations tend to be active at the onset of sequences during replay, it is relevant that deep CA1 cells contribute most of the projections to brain areas involved with goal and reward, such as the nucleus accumbens, prefrontal cortex and septal area (Slomianka *et al.*, 2011). In contrast, cells that become activated later in the sequence tend to encode earlier parts of the journeys to the reward, and superficial CA1 neurons project mainly to the entorhinal cortex (Slomianka *et al.*, 2011). Hence, a gradual shift of activity from deep to superficial CA1 cells may allow a gradual decrease of CA1 input to reward centers during replay, as the encoded positions of replayed cells move further away from the reward. This mechanism would be of manifest importance for learning and memory of reward locations.

Finally, our data must be interpreted with caution because they were obtained from *in vitro* hippocampal slices prepared from juvenile rats. Juvenile preparations are necessary for our work because more mature CA3 neurons (but not CA1 neurons) can only be sparsely loaded with calcium indicators for unknown reasons. In the intact adult hippocampus, CA3 pyramidal cells elongate their axons extensively to the CA1 region along the longitudinal axis of the hippocampus in a three-dimensional manner (Ishizuka *et al.*, 1990), and the axon of even a single CA3 pyramidal cell is highly arborized, covering two-thirds of the septotemporal CA1 region (Li *et al.*, 1994). Further investigations using more intact and adult preparations will facilitate a more comprehensive understanding of hippo-

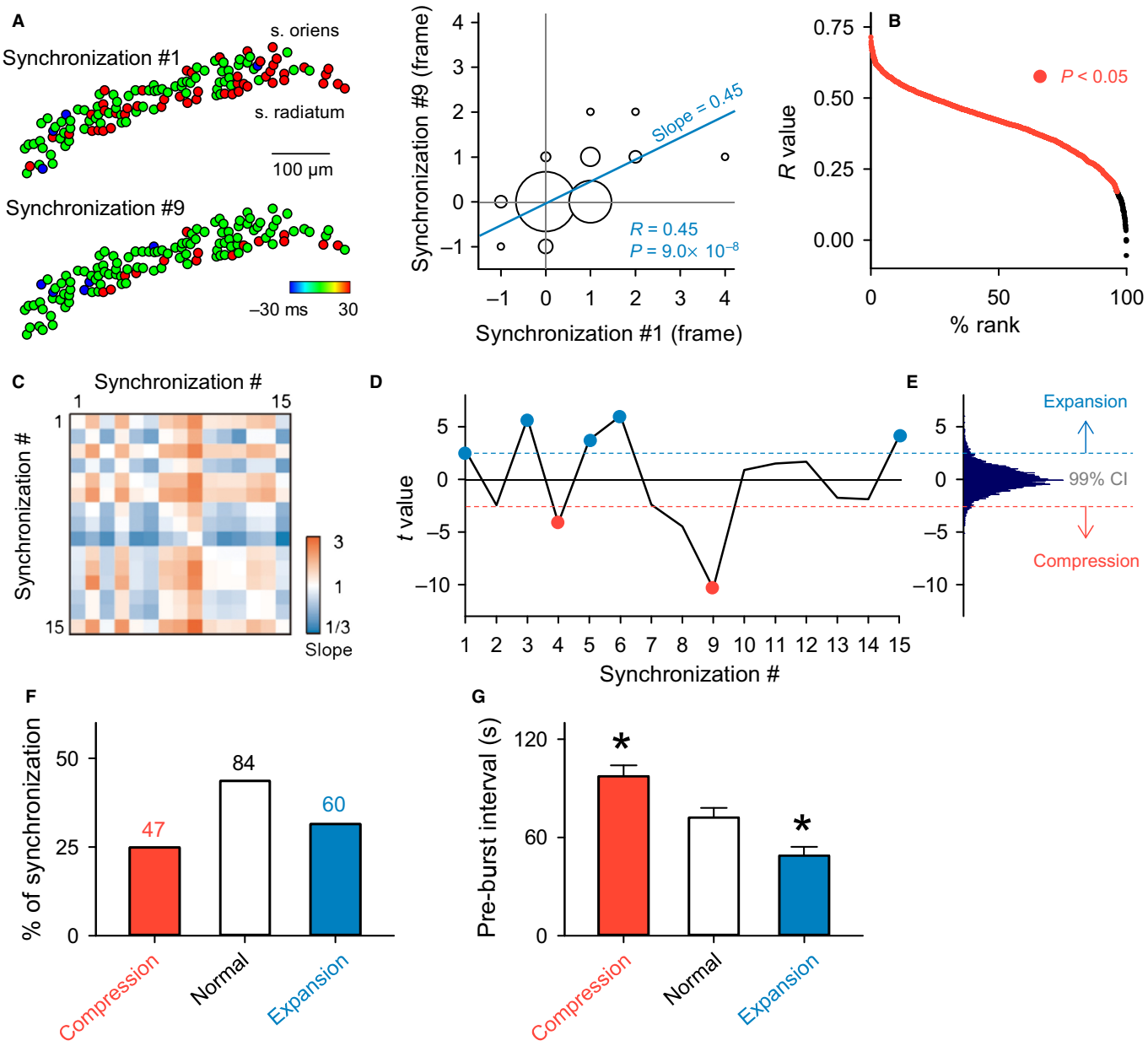

FIG. 7. Temporal flexibility of the neuronal sequences during the synchronized bursts. (A) For two representative synchronous bursts (events #1 and #9) in a slice, the activation timings of the individual neurons are compared in cell maps (left) and a pairwise correlation plot (right). The correlation efficient was 0.45 in the linear regression analysis ($P = 9.0 \times 10^{-8}$). The slope of the regression line (blue line) in the correlation plot was 0.45, indicating that the sequential activation of event #9 was faster than that of event #1. The sizes of the circles represent the number of neurons. (B) Distribution of the correlation coefficients (R) of all 2064 possible pairs in 193 synchronous events from 10 slices. The red dots indicate the event pairs with statistically significant regressions. (C) All possible pairs of 15 synchronous events in the same slice as A were analysed using linear regression analysis, and their slopes are shown in a pseudocolored scale. (D) The t-value of each synchronous event was computed from the total distribution of the slopes in the same slice as C. The red and blue dots indicate synchronous events with sequential neuron activation speeds that were significantly faster (time-compression) or slower (time-expansion) than the average speed. (E) The 1% significance levels of the slopes were determined in the chance distribution estimated by 1000 surrogates, in which the slopes were randomly shuffled in the matrix in C. (F) A total of 191 synchronous events from 10 slices were divided into compressed, normal, and expanded temporal patterns. (G) The mean ± SEM intervals between the focused events and the immediately preceding events. Neuronal sequences that occurred after a longer silent period occurred more quickly. *$P < 0.05$ vs. normal, Dunnett's test after one-way ANOVA. CI, confidence interval.

campal processing. We believe that the present study represents the first step in this process.

Acknowledgements

We thank Mr Takeyuki Miyawaki for his comments on an early version of this article. This work was supported by Kakenhi (25119004) and Health and Labour Sciences Research Grants for Research on Regulatory Science of Pharmaceuticals and Medical Devices from MHLW (iNCENS).

Abbreviation

aCSF, artificial cerebrospinal fluid.

References

Amaral, D. & Lavanex, P. (2007) Hippocampal neuroanatomy. In Andersen, P.M.R., Amaral, D, Bliss, T & O'Keefe, J (Eds), *The Hippocampus Book*. Oxford University Press, Oxford, pp. 37–114.

Baimbridge, K.G., Peet, M.J., McLennan, H. & Church, J. (1991) Bursting response to current-evoked depolarization in rat CA1 pyramidal neurons is correlated with lucifer yellow dye coupling but not with the presence of calbindin-D28k. *Synapse*, **7**, 269–277.

Diba, K. & Buzsaki, G. (2007) Forward and reverse hippocampal place-cell sequences during ripples. *Nat. Neurosci.*, **10**, 1241–1242.

Dragoi, G. & Tonegawa, S. (2011) Preplay of future place cell sequences by hippocampal cellular assemblies. *Nature*, **469**, 397–401.

Druckmann, S., Feng, L., Lee, B., Yook, C., Zhao, T., Magee, J.C. & Kim, J. (2014) Structured synaptic connectivity between hippocampal regions. *Neuron*, **81**, 629–640.

Girardeau, G., Benchenane, K., Wiener, S.I., Buzsaki, G. & Zugaro, M.B. (2009) Selective suppression of hippocampal ripples impairs spatial memory. *Nat. Neurosci.*, **12**, 1222–1223.

Graves, A.R., Moore, S.J., Bloss, E.B., Mensh, B.D., Kath, W.L. & Spruston, N. (2012) Hippocampal pyramidal neurons comprise two distinct cell types that are countermodulated by metabotropic receptors. *Neuron*, **76**, 776–789.

Hopfield, J.J. (1982) Neural networks and physical systems with emergent collective computational abilities. *Proc. Natl. Acad. Sci. USA*, **79**, 2554–2558.

Ishizuka, N., Weber, J. & Amaral, D.G. (1990) Organization of intrahippocampal projections originating from CA3 pyramidal cells in the rat. *J. Comp. Neurol.*, **295**, 580–623.

Kendall, M.G., Stuart, A., Ord, J.K., Arnold, S.F. & O'Hagan, A. (1994) *Kendall's Advanced Theory of Statistics*. Halsted Press, New York.

de Lavilleon, G., Lacroix, M.M., Rondi-Reig, L. & Benchenane, K. (2015) Explicit memory creation during sleep demonstrates a causal role of place cells in navigation. *Nat. Neurosci.*, **18**, 493–495.

Lee, A.K. & Wilson, M.A. (2002) Memory of sequential experience in the hippocampus during slow wave sleep. *Neuron*, **36**, 1183–1194.

Li, X.G., Somogyi, P., Ylinen, A. & Buzsaki, G. (1994) The hippocampal CA3 network: an in vivo intracellular labeling study. *J. Comp. Neurol.*, **339**, 181–208.

Liao, D., Hessler, N.A. & Malinow, R. (1995) Activation of postsynaptically silent synapses during pairing-induced LTP in CA1 region of hippocampal slice. *Nature*, **375**, 400–404.

Mizuseki, K., Diba, K., Pastalkova, E. & Buzsaki, G. (2011) Hippocampal CA1 pyramidal cells form functionally distinct sublayers. *Nat. Neurosci.*, **14**, 1174–1181.

Nakashiba, T., Young, J.Z., McHugh, T.J., Buhl, D.L. & Tonegawa, S. (2008) Transgenic inhibition of synaptic transmission reveals role of CA3 output in hippocampal learning. *Science*, **319**, 1260–1264.

Nakashiba, T., Buhl, D.L., McHugh, T.J. & Tonegawa, S. (2009) Hippocampal CA3 output is crucial for ripple-associated reactivation and consolidation of memory. *Neuron*, **62**, 781–787.

Sasaki, T., Takahashi, N., Matsuki, N. & Ikegaya, Y. (2008) Fast and accurate detection of action potentials from somatic calcium fluctuations. *J. Neurophysiol.*, **100**, 1668–1676.

Sasaki, T., Matsuki, N. & Ikegaya, Y. (2012) Heterogeneity and independency of unitary synaptic outputs from hippocampal CA3 pyramidal cells. *J. Physiol.*, **590**, 4869–4880.

Scheffer-Teixeira, R., Belchior, H., Caixeta, F.V., Souza, B.C., Ribeiro, S. & Tort, A.B. (2012) Theta phase modulates multiple layer-specific oscillations in the CA1 region. *Cereb. Cortex*, **22**, 2404–2414.

Schmidt, H. (2012) Three functional facets of calbindin D-28k. *Front. Mol. Neurosci.*, **5**, 25.

Slomianka, L. (1992) Neurons of origin of zinc-containing pathways and the distribution of zinc-containing boutons in the hippocampal region of the rat. *Neuroscience*, **48**, 325–352.

Slomianka, L., Amrein, I., Knuesel, I., Sorensen, J.C. & Wolfer, D.P. (2011) Hippocampal pyramidal cells: the reemergence of cortical lamination. *Brain Struct. Funct.*, **216**, 301–317.

Sorensen, J.C., Tonder, N. & Slomianka, L. (1993) Zinc-positive afferents to the rat septum originate from distinct subpopulations of zinc-containing neurons in the hippocampal areas and layers. A combined fluoro-gold tracing and histochemical study. *Anat. Embryol.*, **188**, 107–115.

Staley, K.J., Longacher, M., Bains, J.S. & Yee, A. (1998) Presynaptic modulation of CA3 network activity. *Nat. Neurosci.*, **1**, 201–209.

Ueno, S., Tsukamoto, M., Hirano, T., Kikuchi, K., Yamada, M.K., Nishiyama, N., Nagano, T., Matsuki, N. & Ikegaya, Y. (2002) Mossy fiber Zn2+ spillover modulates heterosynaptic N-methyl-D-aspartate receptor activity in hippocampal CA3 circuits. *J. Cell Biol.*, **158**, 215–220.